doi:10.1016/j.carbon.2010.01.063

Toughening and hardening in double-walled carbon nanotube/nanostructured magnesia composites

Alain Peigney [*], *Felipe Legorreta Garcia* [1], *Claude Estournès*, *Alicia Weibel*, *Christophe Laurent*

Université de Toulouse, Institut Carnot CIRIMAT, UPS CNRS, Université Paul-Sabatier, 118 route de Narbonne, 31062 Toulouse cedex 9, France

A B S T R A C T

Dense double-walled carbon nanotube (DWCNT)/nanostructured MgO composites were prepared using an *in situ* route obviating any milling step for the synthesis of powders and consolidation by spark-plasma-sintering. An unambiguous increase in both toughness and microhardness is reported. The mechanisms of crack-bridging on an unprecedented scale, crack-deflection and DWCNT pullout have been evidenced. The very long DWCNTs, which appear to be mostly undamaged, are very homogeneously dispersed at the grain boundaries of the matrix, greatly inhibiting the grain growth during sintering. These results arise because the unique microstructure (low content of long DWCNTs, nanometric matrix grains and grain boundary cohesion) provides the appropriate scale of the reinforcement to make the material tough.

1. Introduction

For over a decade, there has been a growing interest in using carbon nanotubes (CNTs) for ceramic–matrix composites applications [1]. For example, CNTs confer an electrical conductivity to a composite with an insulating matrix such as Al_2O_3 [2–4] or $MgAl_2O_4$ [5], with a very low loading (<1 vol.%) owing to their very high aspect ratio (>10,000), which allows their electrical percolation at a very low content. However, one of the most elusive and controversial issue has been that of toughening. Although a toughness increase has been reported [6–17] from indentation-derived values, authors using macroscopic methods, i.e. using notched specimen, rarely reported a significant increase [18] but most often either a very moderate increase [19–21] or no increase at all [2,22–25]. It has been proposed [22,26–28] that toughness for CNT–ceramic composites should indeed be measured by macroscopic methods and that indentation-derived values are overestimated, notably because such composites are highly resistant to damage contact [22,27]. It was recently stressed [28] that the mechanistic origins of any actual toughness enhancement that may exist in these materials still stand. It is important to note that the presence of CNTs induce changes in the sintering kinetics and mechanisms [29], which can greatly modify the matrix microstructure [2]. This may in turn have a greater effect on the properties than the actual presence of CNTs [27]. Moreover, different kinds of CNTs, such as single-, double- and multi-walled CNTs (SWCNTs, DWCNTs and MWCNTs, respectively), could also produce different microstructures due to their difference in aspect ratio, defect proportion, mechanical properties and tendency to gather into bundles. DWCNTs are a unique class of CNTs, with a formation mechanism similar to SWCNTs [30,31], and are possibly more interesting for composite applications because the outer wall could interact with the matrix, and also protect the inner wall from any damage. Here we report for the first time a strong, unambiguous, increase in both toughness and microhardness for DWCNT–MgO composites. The

[*] *Corresponding author:* Fax: +33 5 61 55 61 63.
E-mail address: peigney@chimie.ups-tlse.fr (A. Peigney).
[1] Present address: Universidad Autonoma del Estado de Hidalgo, Hidalgo, Mexico.
0008-6223/$ - see front matter

composite powders were prepared by an *in situ* catalytic chemical vapor deposition (CCVD) route [32], without any mixing or milling, thus avoiding any CNT damage at this step and ensuring optimal dispersion of the DWCNTs. The materials were densified by spark-plasma-sintering (SPS). The DWCNTs produce a unique microstructure and we argue that a combination of microstructural features, crack-deflection at the DWCNT/matrix interface, DWCNT pullout on the fracture surfaces and large-scale crack-bridging by the DWCNTs do contribute to the high toughness and microhardness.

2. Experimental methods

2.1. Powder synthesis

Powders of MgO and of the $Mg_{0.99}(Co_{0.75}Mo_{0.25})_{0.01}O$ catalytic material were prepared by the combustion route using citric acid as the fuel and the appropriate amounts of $Mg(NO_3)_2{\cdot}6H_2O$, $Co(NO_3)_3{\cdot}9H_2O$ and $(NH_4)_6Mo_7O_{24}{\cdot}4H_2O$. We used a muffle furnace preheated at 550 °C and operated with the door open in normal laboratory atmosphere. Six grams of powder were prepared in one combustion batch. The $Mg_{0.99}(Co_{0.75}Mo_{0.25})_{0.01}O$ powder was divided into two batches, which were submitted to a CCVD treatment in H_2–CH_4 atmosphere with different experimental conditions (950 °C-15 mol.% CH_4 and 1000 °C-20 mol.% CH_4) in order to produce two composite powders with a different carbon content. The gas flow was dried on P_2O_5. Its composition and flow (15 L/min) was monitored using a massflow controller. Heating and cooling rates were equal to 5 °C/min and no dwell was applied at the maximum temperature.

2.2. Spark-plasma-sintering

The sintering was performed by SPS (Dr. Sinter 2080, SPS Syntex Inc., Japan). Samples of the powders were loaded into a 20 mm inner diameter graphite die. A sheet of graphitic paper was placed between the punch and the powder as well as between the die and the powder for easy removal. The powders were sintered in a vacuum (residual cell pressure <3 Pa). A pulse configuration of 12 pulses (one pulse duration 3.3 ms) followed by 2 periods (6.6 ms) of zero current was used. Heating rates of 150 °C/min and 100 °C/min were used from room temperature to 600 °C and from 600 to 1650 °C, respectively, where a 5 min dwell was applied. An optical pyrometer, focused on a little hole at the surface of the die, was used to measure the temperature. A uniaxial charge (corresponding to 150 MPa) was applied from 1000 °C upwards and maintained during the dwell. Natural cooling was applied down to room temperature. The uniaxial pressure was gradually released during cooling. Final sintered specimen size was 20 mm diameter pellets with a thickness of 2.5 mm. The sintered pellets were polished with a diamond paste up to 0.5 μm.

2.3. Microstructure characterization

The carbon content in the powders was determined by flash combustion with an accuracy of 2%. The specific surface area was measured by the BET method using N_2 adsorption at liquid-N_2 temperature (Micromeritics FlowSorb II 2300). The reproducibility of the results is ±3%. Raman spectra for the powders and on the polished surface of sintered materials were obtained with a Jobin-Yvon LabRAM HR 800 (laser excitation at 632 nm). Three Raman spectra were averaged for each sample. The density of the pellets was measured by the Archimedes method. The relative densities ($\rho \pm 0.6\%$) were calculated using 1.80 for DWCNTs and supposing that cobalt and molybdenum species, which account for very small quantities, are present as metallic Co and Mo_2C, respectively. The powders and sintered materials were observed by field-emission-gun scanning electron microscopy (FESEM, JEOL JSM 6700F) and transmission electron microscopy (TEM, JEOL JEM 2100F). The samples of sintered materials for TEM observations were prepared using a grinding, dimpling and ion-milling routine.

2.4. Electrical and mechanical testing

The electrical conductivity was measured at room temperature with d.c. currents on parallelepipedic specimens ($1.6 \times 1.6 \times 8\ mm^3$), parallel to their length, i.e. perpendicular to the pressing axis. The values were rounded to the nearest S/cm. The current densities used were lower than 160 mA/cm^2 (Keithley 2400). The indentation tests were performed (5 N for 10 s in air at room temperature) on the polished surface of the specimens by loading with a Vickers indenter (Shimadzu HMV 2000). The corresponding diagonals of the indentation were measured using an optical microscope attached to the indenter. The fracture strength was measured by the three-point bending method on specimens about $1.8 \times 1.8 \times 18\ mm^3$ machined with a diamond saw. The toughness was calculated from three-point bending results on notched specimens (single-edge notch beam, SENB) using a calibration factor [33]. A notch about half the thickness of the specimen was made using a 100 μm diameter SiC wire.

3. Results and discussion

3.1. Composite powders

The two composite powders produced by using CCVD treatment with different conditions (950 °C-15 mol.% CH_4 and 1000 °C-20 mol.% CH_4) show carbon contents $C_n = 2.3$ and 7.1 wt.%, respectively. These powders will be referred to as P2 and P7, respectively. The increase in C_n is matched by an increase of the specific surface area (71 and 117 m^2/g for P2 and P7, respectively), showing that it corresponds to an increase in the content of CNTs, because the CNTs contribute much to the specific surface area of the powder [34]. A typical FESEM image for P2 (Fig. 1a) reveals bundles of CNTs dispersed in the MgO micrometric agglomerates made up of MgO grains, most being not larger than 30 nm. Both the quantity of bundles and their diameter increase with the CNTs content. For P7 (Fig. 1b), the bundle diameter can reach 50 nm and their length tens or even hundreds of micrometers. A typical TEM image (Fig. 1c) reveals that the MgO crystallites are cubic and below 20 nm in size. Individual CNTs,

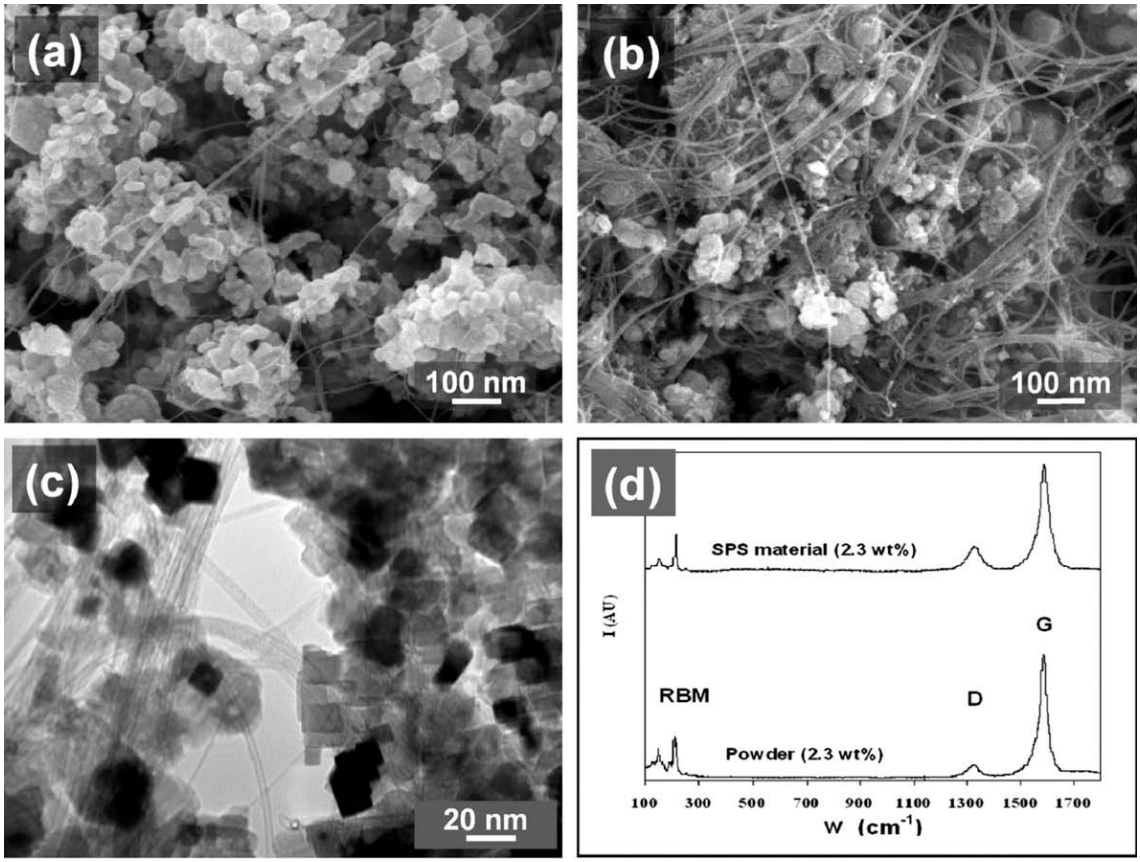

Fig. 1 – FESEM images of the DWCNT–MgO powders P2 (a) and P7 (b); a typical TEM image (c) and Raman spectra of the P2 powder and the sintered S2 composite (d).

either isolated or in bundles, are also observed. An earlier study [35] revealed that about 80% of the CNTs are DWCNTs (with 15% single- and 5% triple-walled CNTs), with outer diameters in the range 1–3 nm and inner diameters in the range 0.5–2.5 nm. The high-frequency range (1100–1800 cm^{-1}) of the Raman spectrum (Fig. 1d) shows the D band (*ca.* 1320 cm^{-1}) and the G band (*ca.* 1589 cm^{-1}). The ratio between the intensity of the D band and G band, $I_{D/G}$, is equal to 0.11 and 0.25 for P2 and P7, respectively. An increasing $I_{D/G}$ value corresponds to a higher proportion of sp^3-like carbon, which is generally attributed to the presence of more structural defects. The radial breathing modes (RBM) are observed in the low-frequency range (100–300 cm^{-1}) of the spectrum. The peak frequencies are inversely proportional to the CNTs diameters. According to calculations, the detected diameters are in the range 0.9–2.2 nm.

3.2. *Sintered materials characteristics*

After sintering by SPS, the produced materials were designated as MgO, S2 and S7. The relative density (Table 1) for MgO is equal to 98.3% and it decreases steadily upon the increase in CNT content, showing that DWCNTs inhibit the densification upon sintering, similarly to SWCNTs [29]. The XRD patterns (not shown) of all composites show the MgO peaks and two weak peaks corresponding to Mo_2C. Metallic cobalt is not detected. The relative proportions of the metal elements in the starting oxide are Mg = 0.99, Co = 0.0075, Mo = 0.0025 and therefore we assume that it is reasonable to consider that the influence of Co and Mo_2C on the properties discussed later is negligible. For S7, a very weak wide peak corresponding to the (0 0 2) graphene planes stacking is detected as well, reflecting the higher DWCNT content. Analysis of the Raman spectrum for S2 (Fig. 1d) reveals that $I_{D/G}$ is equal to 0.24, which only slightly higher than for the corresponding powder ($I_{D/G}$ = 0.11), reflecting the presence of more structural defects in the DWCNTs. However, both this moderate increase and the presence of RBM peaks indicate only minor damages to the DWCNTs. No shift of the G band is observed as compared with the powder, which could indicate that no thermal residual stresses have developed after cooling down from the sintering temperature, in contrast to results reported for alumina–matrix composites [9] or DWCNTs–SiO_2 composites [36]. However, the presence of thermal stresses in the bulk of the material can not be ruled out because the polishing of the samples could contribute to relax the residual stresses at the surface. In order to further evaluate the degree of damage, a piece of S2 was soaked overnight in a concentrated HCl aqueous solution in order to dissolve the MgO matrix and the resulting material was observed by TEM, revealing many individual undamaged CNTs (Supplementary Information 1). FESEM images of fracture surfaces

Table 1 – Characteristics and properties of the materials prepared by SPS: C_n: carbon content; d: MgO matrix grain size; ρ: relative density; HV: Vickers microhardness, σ_f: fracture strength and K_{Ic}: SENB toughness (the average, minimum/maximum values are indicated); σ: electrical conductivity (minimum and maximum values).

	C_n (wt.%)	d (nm)	ρ (%)	HV (GPa)	σ_f (MPa)	K_{Ic} (MPa $m^{1/2}$)	σ (S cm^{-1})
MgO	0	31,000	98.3	7.5 (6.9/8.1)	91 (89/93)	3.4 (3.3/3.5)	0
S2	2.3	200	96.3	12.2 (10.8/15.3)	276 (170/377)	6.7 (6.2/7.5)	1.9–2.1
S7	7.1	60–70	93.4	7.4 (5.8/8.8)	218 (187/251)	3.1 (2.4/4.1)	6.3–6.9

clearly reveal that the MgO grain size dramatically decreases upon the increase in CNT content, from 31 μm for MgO (Fig. 2a) to only 200 nm for S2 (Fig. 2b) and 60–70 nm for S7 (Fig. 2d). These sizes were confirmed by images of polished surfaces (Supplementary Information 2). Interestingly, for S7, the MgO grain size is only slightly larger to that in the powder, showing that grain growth was greatly inhibited. For the two composites, homogenously-distributed CNTs are observed on the fracture surfaces and the fracture seems to be intergranular, in line with the low matrix grain size (⩽200 nm). Fracture surface images for S2 will be discussed in more details later. The CNTs appear to be undamaged and their apparent quantity is well correlated to the carbon content. However, higher-magnification images (Fig. 2c) show the presence of nanometric clusters at the matrix grain junctions, which could reflect that a small proportion of the CNTs, probably individual DWCNTs, have been damaged. HRTEM observations of S2 (Fig. 3a) and S7 (Fig. 3b) confirm the matrix grain size evaluated from the FESEM observations and also reveal another important difference: CNTs are observed at only some of the grain boundaries or grain junctions for S2, but by contrast they are observed at all grain boundaries for S7, the bundles forming an interphase about 10 nm across. Thus, in S2, large areas of grain boundaries are free of DWCNTs whereas in S7, individual or bundled DWCNTs are segregated at most grain boundaries areas, which does greatly inhibit the grain growth and is detrimental to the grain boundary cohesion. The segregation of SWCNTs bundles at the grain boundaries was already observed for SWCNTs–Al_2O_3 composites [7,8,22,37–40]. A typical higher magnification image (Fig. 3c) reveals fringes corresponding to a fairly well-organized bundle of CNTs, oriented uniformly and lying flat on the MgO

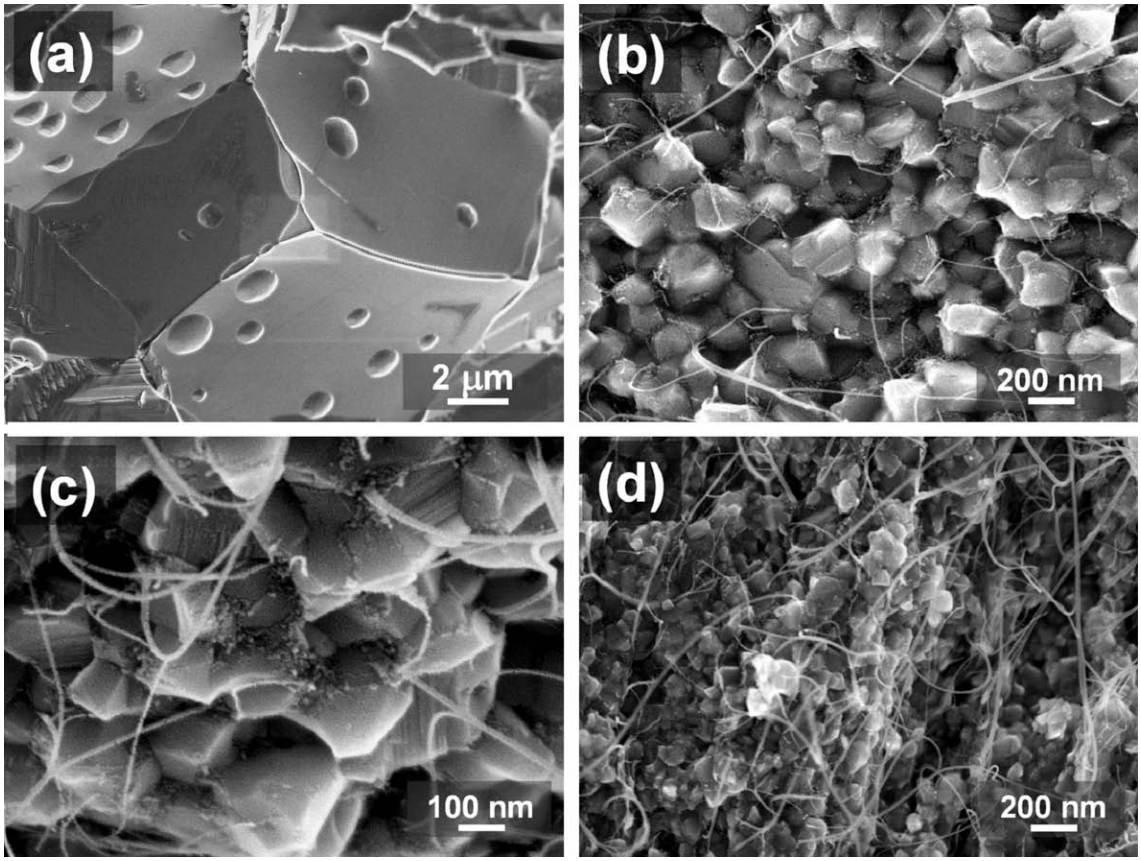

Fig. 2 – FESEM images of the fracture surface of MgO (a), S1 (b and c) and S7 (d).

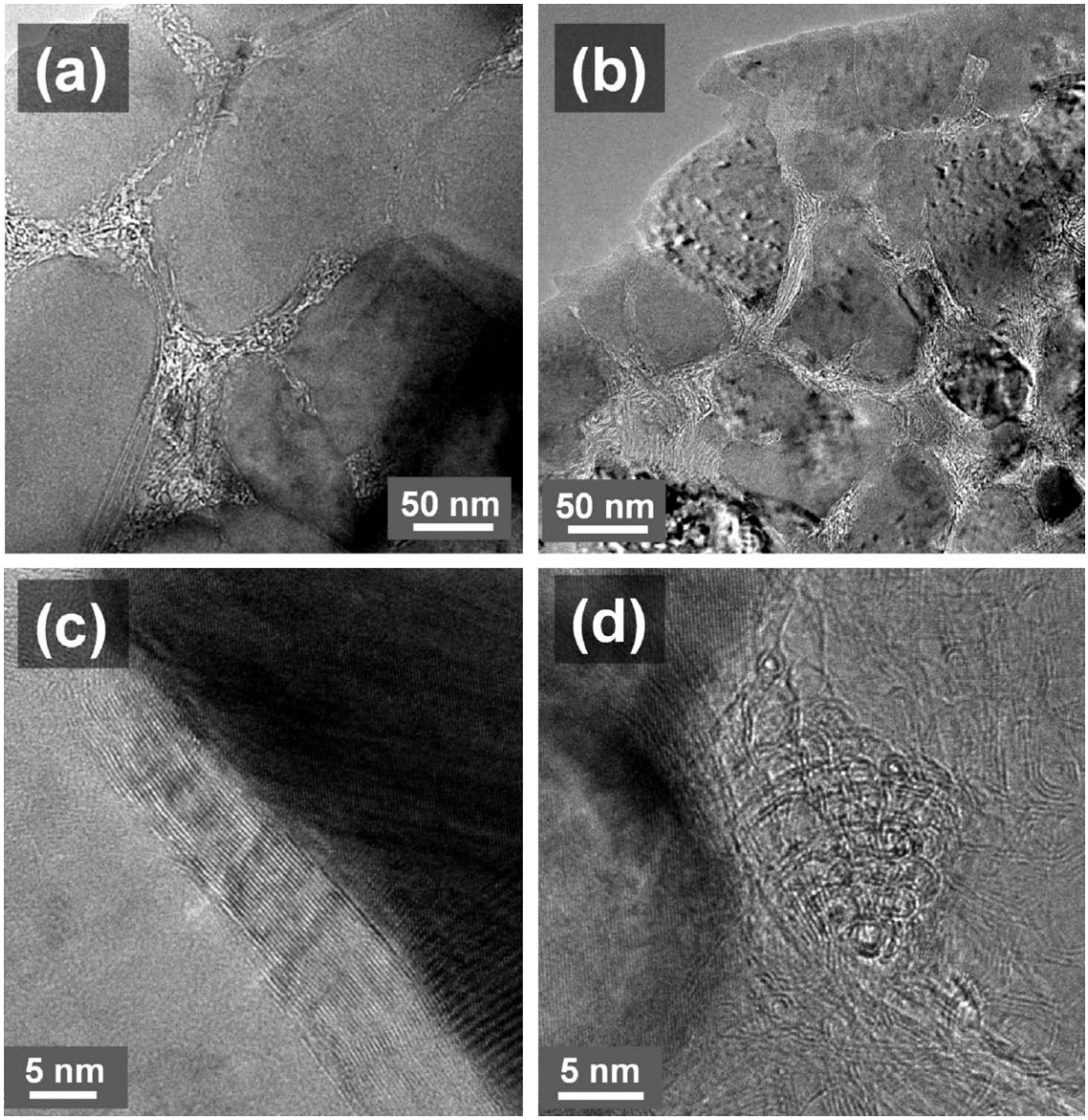

Fig. 3 – HRTEM images showing the grain boundaries in S2 (a) and S7 (b) and typical higher-magnification images (c, d).

grain. In some areas (Fig. 3d), the DWCNTs walls have been resolved, showing the two walls on both sides along the CNT axis. Moreover, double concentric ring patterns reflect DWCNTs in the bundles that have intersected the surface edge-on. These observations confirm that there is no widespread degradation of the DWCNTs, in good agreement with the above Raman spectroscopy results and the TEM observation of DWCNTs after the dissolution of the matrix. This is in sharp contrast with our earlier results where the CNT–MgO composites were sintered by hot-pressing [2]. This may be due to the shorter duration when using SPS and also to the better quality of the present DWCNTs.

3.3. *Electrical conductivity and mechanical properties*

The electrical conductivity, Vickers microhardness, fracture strength and toughness are reported in Table 1. It was verified that MgO is insulating. The electrical conductivity for the S2 and S7 composites (1.9–6.9 S cm^{-1}, respectively) increases upon the increase in DWCNTs content. These values are in line with results reported for other CNT-oxide composites [2–5,8,37,41,42]. The Vickers microhardness for S2 (12.2 GPa) is significantly higher than the values found for MgO and S7 (7.5 and 7.4 GPa, respectively). The value for S2 was checked for three different pellets, with 15 measures each. The influence of CNTs on the microhardness of CNT-oxide composites is not clearly established in the literature but the method by which the composite powder is prepared appears to be very important. Indeed, when starting from powders prepared by mechanical mixing of powders or powder suspensions, it was reported [9,10,25,43] that the microhardness decreases with increasing proportions of CNT bundles, which was related to the simultaneous decrease in relative density. By contrast, An et al. [17,44] have used a method where CNTs are

formed *in situ* in an Al_2O_3 matrix, i.e. a route roughly similar to the present one, and have reported a regular increase in microhardness when the CNTs content was increased up to 4 wt.%. This was related to a lower matrix grain size, but without ruling out a possible CNTs reinforcement effect. Other researchers [15,16] have used methods where the matrix is synthesized *in situ* around the CNTs and have also reported that the microhardness increases up to a certain CNTs fraction but that CNTs agglomeration for higher loadings causes a decrease. These researchers [15,16] proposed that owing to their particular powder preparation route, as opposed to mechanical mixing, the CNTs were well-dispersed within, and strongly bonded with the alumina grains, which made possible an effective load transfer from the matrix grains to the CNTs. Thus, it is possible that in the present case, the higher microhardness observed for S2 could reflect the grain size refinement discussed above and also a good bonding between the DWCNTs and the MgO grains. The decrease for S7 could reflect its lower relative density (only 93.4%) and a poor cohesion of the grain boundaries due the presence of a DWCNTs inter granular phase and the very moderate MgO grain growth during the sintering.

For MgO, the fracture strength (91 MPa) is lower, and the toughness (3.4 MPa $m^{1/2}$) is higher, than the values (230 MPa and 2.2 MPa $m^{1/2}$, respectively) reported [45] for a MgO material with the same grain size. For S2 and S7, the fracture strength is in line with the reported [45] value. The toughness for S7 (3.9 MPa $m^{1/2}$) is similar to that for the present MgO but interestingly the toughness for S2 (6.7 MPa $m^{1/2}$) is markedly higher, almost double. Several points will be discussed before studying S2 into more details. Considering that for all materials the notches were made using a 100 μm diameter SiC wire, the classical effect [46] of an artificially high toughness being due to crack initiation at a blunt, uncontrolled notch root is ruled out. For the higher DWCNT content (S7), as mentioned above, the DWCNTs form a 10 nm interphase at the MgO grain boundaries and the growth of the MgO grain during sintering was very moderate. Consequently, we infer that in S7 most of the grains boundaries have a poor cohesion. It should also be noted that during the preparation of the S7 test samples, several of them separated into flakes due to a delamination of the material. An accumulation of DWCNTs could be highlighted on the surfaces of the flakes. The handling of the composite powders with a high DWCNTs content could result in a tangling of the bundles, which would thus form large agglomerates which upon compaction are crushed and create barriers between groups of matrix grains, perpendicular to the compaction axis. Poorly cohesive areas are thus created, which are likely to provoke the sample delamination under shear stresses during polishing or machining. Thus, a too high DWCNT content is to be avoided. FESEM images of the fracture surface of a S2 sample which was broken during the mechanical test (Fig. 4a and b) confirm that the fracture is mostly intergranular although some transgranular fracture is also observed. Several DWCNT bundles are protruding from the surface, and some bundles are cut near the grain surface, suggesting some degree of bundle pullout, as was observed before for CNT–Al_2O_3 composites [2,11,15,17,20,23,24,47,48]. Vickers patterns were made using a deliberately high load (1 kg) in order to produce cracks. Crack-deflection is observed (Fig. 4c) along the MgO grain boundaries due to the low MgO grain size, in line with the mostly intergranular fracture. Few crack-bridging by the DWCNTs is observed when the crack width is below 100 nm (white arrows in Fig. 4d and e). By contrast, crack-bridging is observed, to a much higher degree than what has been reported before [9,10,15,16,20,21,27,48], when the crack width is in the range 300–500 nm, i.e. farther away from the crack tip (Fig. 4f and g). The fact that less DWCNTs are observed in narrower parts of cracks (Fig. 4d and e) compared to other areas (Fig. 4f and g) can be firstly explained by their superimposition with matrix grains which gives image contrasts unfavourable to their imaging. Moreover, in their narrower part, cracks have also a low depth and electron edge-effect of matrix grains, some also bridging the cracks, could be mistakenly interpreted as CNTs. Secondly, most DWCNTs are neither aligned nor stressed initially in the material but are located along the MgO grain boundaries and are flexible enough to closely follow the grain surfaces. Thus, these CNTs become fully deployed in areas where the crack is quite wide already and consequently are imaged in higher quantities. Most DWCNTs appear to be taught, i.e. under tensile stress, but some are broken. Thus, CNTs are not free to slide easily within the matrix which reflects the existence of a load transfer between CNTs and the matrix. We rule out the possibility of a chemical bonding because of the very improbable local carburization of MgO. However, SEM and TEM observations showed that there is a good wetting of CNTs by the matrix and also that CNTs or CNT bundles are mainly located at the matrix grain boundaries and consequently have a very sinuous shape. Because of their very high aspect ratio (more than 10,000), and owing to their high aptitude to elastic deformation (i.e. reversible, without damages), a huge quantity of successive deformations are involved during the sliding of a CNT or a CNTs bundle in its sinuous path. This requires a significant energy, which, taking into account the great quantity of CNTs, could greatly contribute to inhibit the crack propagation. Thus, reinforcement mechanisms can not be compared with those involved in classical long fiber ceramic composites because of the great difference of scales, of filament organization and of filaments characteristics and mechanical properties. It is probable that the DWCNTs directly contribute to the reinforcement, but that their action is higher in areas where the crack is quite wide already. During crack propagation, mostly by decohesion at the grain boundaries, the DWCNTs are progressively unfolded and taught one after the other as the crack widens, because of the mechanical locking by adjacent MgO grains, thus ensuring some load transfer. At a certain point, all the DWCNTs which were thus unfolded do bridge the crack. Some bridging DWCNTs are broken, therefore absorbing a fraction of the fracture energy. The elastic deformation energy absorbed by one DWCNT for unfolding is weak but one could think that the cumulated energy necessary for the fracture of all the bridging DWCNTs is much higher and thus this is likely to limit the crack propagation. Many authors have conducted modelling or experimental works on MWCNT

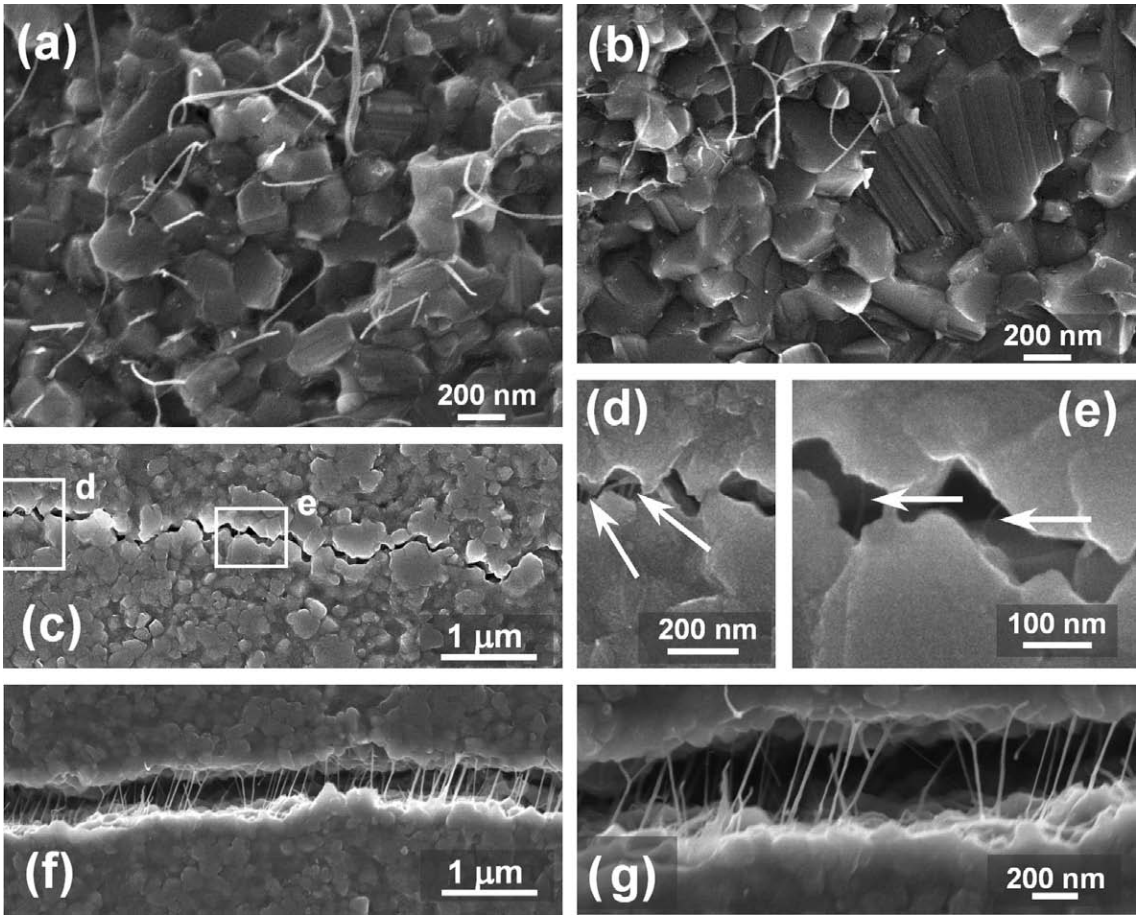

Fig. 4 – FESEM images of S2 showing fracture surfaces (a and b), a crack with a width below 100 nm where appears the crack-deflection by matrix grains (c), two details of the previous crack bridged by a few DWCNTs, at a higher magnification (d–e), and a 300–500 nm wide crack bridged by many DWCNTs (f and g).

deformation and fracture and some have focused on DWCNTs [49–53], showing that the advantages of using DWCNTs rather than SWCNTs are debatable, particularly because of the low friction on intertube sliding. Recently, Byrne et al. [54] and Li et al. [53], using molecular dynamics modelling, underligned that interwall sp^3 bonding would greatly improve the sliding resistance in MWCNTs or DWCNTs, which could be of first importance in the case of CNT–ceramic composites. Peng et al. [55] showed that such interwall sp^3 bonding can be obtained by electron irradiation, which was not performed here. The possible occurrence of such bonds in the present materials was not investigated for the present work and could represent a further study. However, during the SPS treatment, high local current densities are probably induced through the sample because of the percolation of the CNTs, and the fact that arc discharges at the CNT–MgO interface could induce interwall bonding can not be ruled out. It has been argued [22] that the fine scale of the SWCNTs as reinforcing elements will result in only small crack-path perturbations and small toughening-zone sizes relative to the crack size, which will render crack-deflection and crack-bridging mechanisms ineffective in SWCNT–Al_2O_3 composites. Here, using undamaged (and hence very long) DWCNTs and strongly limiting the matrix grain growth during SPS provides the appropriate scale of the reinforcement to make the material tough.

4. Conclusion

A strong, unambiguous, increase in both toughness and microhardness for ceramic–matrix composites reinforced with DWCNTs is reported for the first time. The mechanisms of crack-bridging on an unprecedented scale, crack-deflection and DWCNT pullout have been evidenced. The DWCNTs, which appear to be mostly undamaged, are very homogeneously dispersed at the grain boundaries of MgO, almost totally preventing grain growth. A too high content of DWCNTs weakens the material. These results arise because of the unique microstructure in terms of DWCNTs length and quality, DWCNT content, matrix grain size and grain boundary structure, achieved through the use of an *in situ* route obviating any milling step for the synthesis of composite powders and through consolidation by SPS.

Acknowledgments

The authors thank L. Datas and L. Weingarten for assistance in the FESEM and HREM observations, which were performed

at TEMSCAN, the "Service Commun de Microscopie Electronique à Transmission", Université Paul-Sabatier (Toulouse). The authors also thank G. Raimbeaux for assistance with the SPS, which was performed at the Plateforme Nationale CNRS de Frittage Flash (PNF^2, Toulouse).

Appendix A. Supplementary data

Supplementary data associated with this article can be found, in the online version, at doi:10.1016/j.carbon.2010.01.063.

REFERENCES

[1] Peigney A, Laurent C. Carbon nanotubes ceramic composites. In: Low IM, editor. Ceramic matrix composites microstructure–property relationship. Cambridge, England: Woodhead Publishing Limited; 2006. p. 309–33.
[2] Flahaut E, Peigney A, Laurent C, Marliere C, Chastel F, Rousset A. Carbon nanotube–metal-oxide composites: microstructure, electrical conductivity and mechanical properties. Acta Mater 2000;48(14):3803–12.
[3] Ahmad K, Pan W, Shi SL. Electrical conductivity and dielectric properties of multiwalled carbon nanotube and alumina composites. Appl Phys Lett 2006;89(13):133122-1–3.
[4] Ahmad K, Pan W. Dramatic effect of multiwalled carbon nanotubes on the electrical properties of alumina based ceramic composites. Compos Sci Technol 2009 Jun;69(7–8):1016–21.
[5] Rul S, Lefevre-schlick F, Capria E, Laurent C, Peigney A. Percolation of single-walled carbon nanotubes in ceramic matrix composites. Acta Mater 2004;52(4):1061–7.
[6] Siegel RW, Chang SK, Ash BJ, Stone J, Ajayan PM, Doremus RW, et al. Mechanical behavior of polymer and ceramic matrix composites. Scr Mater 2001;44(8/9):2061–4.
[7] Zhan G-D, Kuntz JD, Wan J, Mukherjee AK. Single-wall carbon nanotubes as attractive toughening agents in alumina-based composites. Nat Mater 2003;2(1):38–42.
[8] Zhan G-D, Mukherjee AK. Carbon nanotube reinforced alumina-based ceramics with novel mechanical, electrical, and thermal properties. Int J Appl Ceram Technol 2004;1(2):161–71.
[9] Jiang D, Thomson K, Kuntz JD, Ager JW, Mukherjee AK. Effect of sintering temperature on a single-wall carbon nanotube-toughened alumina-based composite. Scripta Mater 2007;56(11):959–62.
[10] Sun J, Gao L, LI W. Colloidal processing of carbon nanotube/alumina composites. Chem Mater 2002;14:5169–72.
[11] Sun J, Gao L, Jin X. Reinforcement of alumina matrix with multi-walled carbon nanotubes. Ceram Int 2005;31(6):893–6.
[12] Ning J, Zhang J, Pan Y, Guo J. Fabrication and mechanical properties of SiO_2 matrix composites reinforced by carbon nanotube, Materials Science and Engineering, A: Structural Materials: Properties, Microstructure and Processing 2003;A357(1–2):392–6.
[13] Ning J, Zhang J, Pan Y, Guo J. Surfactants assisted processing of carbon nanotube-reinforced SiO_2 matrix composites. Ceram Int 2004;30(1):63–7.
[14] Lim DS, You DH, Choi HJ, Lim SH, Jang H. Effect of CNT distribution on tribological behavior of alumina–CNT composites. Wear 2005;259(1–6):539–44.
[15] Cha SI, Kim KT, Lee KH, Mo CB, Hong SH. Strengthening and toughening of carbon nanotube reinforced alumina composite fabricated by molecular level mixing process. Scr Mater 2005;53(7):793–7.
[16] Mo CB, Cha SI, Kim KT, Lee KH, Hong SH. Fabrication of carbon nanotube reinforced alumina matrix composite by sol–gel process, Materials Science and Engineering, A: Structural Materials: Properties, Microstructure and Processing 2005;A395(1–2):124–8.
[17] Zhang T, Kumari L, Du GH, Li WZ, Wang QW, Balani K, et al. Mechanical properties of carbon nanotube–alumina composites synthesized by chemical vapor deposition and spark plasma sintering. Compos Part A-Appl Sci Manuf 2009;40(1):86–93.
[18] Fan JP, Zhuang DM, Zhao DQ, Zhang G, Wu MS, Wei F, et al. Toughening and reinforcing alumina matrix composite with single-wall carbon nanotubes. Appl Phys Lett 2006;89(12):121910-1–3.
[19] Fan J, Zhao D, Wu M, Xu Z, Song J. Preparation and microstructure of multi-wall carbon nanotubes-toughened Al_2O_3 composite. J Am Ceram Soc 2006;89(2):750–3.
[20] Yamamoto G, Omori M, Hashida T, Kimura H. A novel structure for carbon nanotube reinforced alumina composites with improved mechanical properties. Nanotechnology 2008;19:315708-1–7.
[21] Ahmad K, Pan W. Hybrid composites: a new route towards tougher alumina ceramics. Compos Sci Technol 2008;68(6):1321–7.
[22] Wang X, Padture NP, Tanaka H. Contact-damage-resistant ceramic/single-wall carbon nanotubes and ceramic/graphite composites. Nat Mater 2004;3(8):539–44.
[23] Laurent C, Peigney A, Dumortier O, Rousset A. Carbon nanotubes Fe alumina composites. Part II: microstructure and mechanical properties of the hot-pressed composites. J Eur Ceram Soc 1998;18(14):2005–13.
[24] Peigney A, Laurent C, Flahaut E, Rousset A. Carbon nanotubes in novel ceramic matrix composites. Ceram Int 2000;26(6):677–83.
[25] Yamamoto G, Omori M, Yokomizo K, Hashida T, Adachi K. Structural characterization and frictional properties of carbon nanotube/alumina composites prepared by precursor method. Mater Sci Eng: B 2008;148(1–3):265–9.
[26] Peigney A. Composite materials: tougher ceramics with nanotubes. Nat Mater 2003;2(1):15–6.
[27] Curtin WA, Sheldon BW. CNT-reinforced ceramics and metals. Mater Today 2004:44–9.
[28] Padture NP, Curtin WA. Comment on "effect of sintering temperature on a single-wall carbon nanotube-toughened alumina-based composite". Scr Mater 2008;58(11):989–90.
[29] Peigney A, Rul S, Lefevre-Schlick F, Laurent C. Densification during hot-pressing of carbon nanotube–metal–magnesium aluminate spinel composites. J Eur Ceram Soc 2007;27(5):2183–93.
[30] Hafner JH, Bronikowski MJ, Azamian BR, Nikolaev P, Rinzler AG, Colbert DT, et al. Catalytic growth of single-wall carbon nanotubes from metal particles. Chem Phys Lett 1998;296(1 and 2):195–202.
[31] Peigney A, Coquay P, Flahaut E, Vandenberghe RE, De Grave E, Laurent C. A study of the formation of single- and double-walled carbon nanotubes by a CVD method. J Phys Chem B 2001;105(40):9699–710.
[32] Flahaut E, Bacsa R, Peigney A, Laurent C. Gram-scale CCVD synthesis of double-walled carbon nanotubes, vol. 12. Cambridge, United Kingdom: Chemical Communications; 2003. p. 1442–3.
[33] Brown WF, Srawley JE. Plane strain crack toughness testing of high strength metallic materials. ASTM Special Technical Publication; 1996. p. 410.
[34] Peigney A, Laurent C, Flahaut E, Bacsa RR, Rousset A. Specific surface area of carbon nanotubes and bundles of carbon nanotubes. Carbon 2001;39(4):507–14.

[35] Flahaut E, Laurent C, Peigney A. Catalytic CVD synthesis of double and triple-walled carbon nanotubes by the control of the catalyst preparation. Carbon 2005;43(2):375–83.
[36] de Andrade MJ, Weibel A, Laurent C, Roth S, Bergmann CP, Estournès C, et al. Electrical conductive double-walled carbon nanotubes – silica glass composites prepared by the sol–gel process and spark plasma sintering. Scr Mater 2009;61(10):988–91.
[37] Zhan G-D, Kuntz JD, Garay JE, Mukherjee AK. Electrical properties of nanoceramics reinforced with ropes of single-walled carbon nanotubes. Appl Phys Lett 2003;83(6):1228–30.
[38] Vasiliev AL, Poyato R, Padture NP. Single-wall carbon nanotubes at ceramic grain boundaries. Scr Mater 2007;56(6):461–3.
[39] Zapata-Solvas E, Poyato R, Gomez-Garcia D, Dominguez-Rodriguez A, Radmilovic V, Padture NP. Creep-resistant composites of alumina and single-wall carbon nanotubes. Appl Phys Lett 2008;92(11):111912-1–3.
[40] Poyato R, Vasiliev AL, Padture NP, Tanaka H, Nishimura T. Aqueous colloidal processing of single-wall carbon nanotubes and their composites with ceramics. Nanotechnology 2006;17(6):1770–7.
[41] Jiang L, Gao L. Carbon nanotubes–magnetite composites from solvothermal processes: formation, characterization, and enhanced electrical properties. Chem Mater 2003;15(14):2848–53.
[42] Liu YQ, Gao L. A study of the electrical properties of carbon nanotube–$NiFe_2O_4$ composites: effect of the surface treatment of the carbon nanotubes. Carbon 2005;43(1):47–52.
[43] Sun J, Gao L, Iwasa M, Nakayama T, Niihara K. Failure investigation of carbon nanotube/3Y-TZP composites. Ceram Int 2005;31(8):1131–4.
[44] An JW, You DH, Lim DS. Tribological properties of hot-pressed alumina–CNT composites. Wear 2003;255(Pt. 1):677–81.
[45] Aksel C, Rand B, Riley FL, Warren PD. Mechanical properties of magnesia–spinel composites. J Eur Ceram Soc 2002;22(5):745–54.
[46] Nishida T, Hanaki Y. Effect of notch-root radius on the fracture toughness of a fine-grained alumina. J Am Ceram Soc 1994;77(2):606–8.
[47] Fan Y-Y, Li F, Cheng H-M, Su G, Yu Y-D, Shen Z-H. Preparation, morphology, and microstructure of diameter-controllable vapor-grown carbon nanofibers. J Mater Res 1998;13(8):2342–6.
[48] Xia Z, Riester L, Curtin WA, Li H, Sheldon BW, Liang J, et al. Direct observation of toughening mechanisms in carbon nanotube ceramic matrix composites. Acta Mater 2004;52(4):931–44.
[49] Ru CQ. Effect of van der Waals forces on axial buckling of a double-walled carbon nanotube. J Appl Phys 2000;87(10):7227–31.
[50] Ru CQ. Axially compressed buckling of a doublewalled carbon nanotube embedded in an elastic medium. J Mech Phys Solids 2001;49(6):1265–79.
[51] Li YJ, Wang KL, Wei JQ, Gu ZY, Wang ZC, Luo JB, et al. Tensile properties of long aligned double-walled carbon nanotube strands. Carbon 2005;43(1):31–5.
[52] Ranjbartoreh AR, Wang GX, Arani AG, Loghman A. Comparative consideration of axial stability of single- and double-walled carbon nanotube and its inner and outer tubes. Physica E 2008;41(2):202–8.
[53] Li LL, Xia ZHH, Curtin WA, Yang YQQ. Molecular dynamics simulations of interfacial sliding in carbon-nanotube/diamond composites. J Am Ceram Soc 2009;92(10):2331–6.
[54] Byrne EM, McCarthy MA, Xia Z, Curtin WA. Multiwall nanotubes can be stronger than single wall nanotubes and implications for composite design. Phys Rev Lett 2009;103(4):045502-1–4.
[55] Peng B, Locascio M, Zapol P, Li SY, Mielke SL, Schatz GC, et al. Measurements of near-ultimate strength for multiwalled carbon nanotubes and irradiation-induced crosslinking improvements. Nat Nanotechnol 2008;3(10):626–31.